Stretchable strain sensor based on $HfSe_2$/LIG composite with high sensitivity and good linearity within a wide range

Yang, Huiru; Wang, Shaogang; Huang, Qianming; Tan, Chunjian; Gao, Chenshan; Xu, Siyuan; Ye, Huaiyu; Zhang, Guoqi

DOI
10.1016/j.apsusc.2023.157772

Publication date
2023

Document Version
Final published version

Published in
Applied Surface Science

Applied Surface Science 636 (2023) 157772

Contents lists available at ScienceDirect

Applied Surface Science

journal homepage: www.elsevier.com/locate/apsusc

Full Length Article

Stretchable strain sensor based on $HfSe_2$/LIG composite with high sensitivity and good linearity within a wide range

Huiru Yang [a,b], Shaogang Wang [c], Qianming Huang [a,b], Chunjian Tan [c], Chenshan Gao [b], Siyuan Xu [b], Huaiyu Ye [b,d,*], Guoqi Zhang [c]

[a] Harbin Institute of Technology, Harbin 150001, China
[b] School of Microelectronics, Southern University of Science and Technology, Shenzhen 518055, China
[c] Faculty of EEMCS, Delft University of Technology, Mekelweg 4, 2628 CD Delft, the Netherlands
[d] College of Optoelectronic Engineering, Chongqing University, Chongqing 400044, China

ARTICLE INFO

Keywords:
$HfSe_2$/LIG composite
Piezoresistive strain sensor
Wearable electronics

ABSTRACT

Flexible strain sensors based on nanomaterials have sparked a lot of interest in the field of wearable smart electronics. Laser induced graphene (LIG) based sensors in particular stand out due to their straightforward fabrication procedure, three-dimensional porous structures, and exceptional electromechanical capabilities. Recent studies have focused on LIG composites, however, it is still difficult to achieve great sensitivity and excellent linearity in a wide linear working range. Herein, a strain sensor with high sensitivity and good linearity is prepared in this work, which was realized by carbonizing the polyimide film coated with $HfSe_2$ to obtain three-dimensional porous graphene nanosheets decorated with $HfSe_2$ ($HfSe_2$/LIG). After being transferred to the flexible substrate of Ecoflex, it exhibits high stretchability, hydrophobicity and robustness, and obtains excellent electromechanical properties. The $HfSe_2$/LIG strain sensor demonstrated high sensitivity (gauge factor, GF ≈ 46), a low detection limit (0.02%), good linearity (R^2 = 0.99) in a large working range (up to 30%), and a quick response time (0.20 s). Additionally, it exhibits good stability and consistent behavior across a large number of strain/release test cycles (>3000 cycles). With these benefits, the sensor can be used to monitor various limb movements (including finger, wrist and neck movements) and minute artery activity, and can generate reliable signals. Therefore, the $HfSe_2$/LIG-based sensor has enormous potential for use in wearable intelligent electronics and movement monitoring.

1. Introduction

Wearable strain sensors have several potential applications in healthcare, [1–4] human-interactive systems, [5,6] and electronic skin [7,8] thanks to their flexibility, high sensitivity, and mechanical robustness. Despite the extensive study in this subject over decades, it remains difficult to build flexible strain sensors with effective and scalable manufacturing methods to achieve ideal stimulation conversion capability and stable signal output over a long working duration. Numerous options have been looked into as the active materials of strain sensors, including metal nanowires [9,10], MXene [11], conductive polymer [12,13], and carbon materials [14,15] (carbon black [16], carbon nanotubes (CNT) [17,18] and graphene [19,20]). Due to their outstanding mechanical and electrical properties, graphene-based materials serve as a typical category of two-dimensional (2D) carbon-based materials and are particularly well suited for strain sensor applications. Han et al. [21] used chemical vapor deposition to product the graphene mesh networks (gauge factor, GF = 2.55 at 70% strain). Stretchable and sensitive strain sensors were created by He et al. [22] using porous polydimethylsiloxane (PDMS) hybrids with CNTs and graphene. Although these sensors based on graphene have excellent sensitivity, graphene materials nevertheless have to deal with difficult preparation procedures and ductility.

The invention of laser-induced graphene (LIG) has created a new method for producing high-performance sensors that is simple, efficient and low-cost manufacturing [23–26]. By directly irradiating carbonaceous precursors, LIG is quickly created and has a porous three-dimensional structure by nature. In sensors, LIG and its variants have found widespread use [24,27,28]. Liu et al. [29] produced porous graphene strain sensors directly on PI fabrics. Kulyk et al. [30] prepared LIG

* Corresponding author at: School of Microelectronics, Southern University of Science and Technology, Shenzhen 518055, China.
E-mail address: yehy@sustech.edu.cn (H. Ye).

https://doi.org/10.1016/j.apsusc.2023.157772
Received 4 April 2023; Received in revised form 15 May 2023; Accepted 10 June 2023
Available online 13 June 2023

flexible sensor on filter paper. These LIG strain sensors fabricated on pristine substrates have certain flexibility and stretchability, however, due to the limited stretchability of the substrate and the weak adhesion of LIG to the substrate, its stretchability range is narrow and its stability is weak. The application potential of LIG is limited by its robustness on substrates. In order to further improve the stability and stretching range of LIG, Tour team [31] developed LIG composites (LIGCs) that are engineered on various substrate by simple infiltration method. Wu et al. [32] fabricated a piezoresistive strain sensor by combining LIG with an elastic substrate (PDMS or Ecoflex), exhibiting a high GF of 37 and a stretch range of 70%. Dallinger et al. [33] prepared highly stretchable (100% strain) and sensitive (GF = 40) strain sensors based on LIG/Polyurethane. These methods improve adhesion and increase the penetration of elastic materials into the carbon network. Therefore, the stretching range of the fabricated strain sensor is widened, but the sensitivity and linearity in a wide range still need to be improved.

Recent research has centered on LIG composites based rare metals. An constructed strain sensor that is loaded with Pt/LIG was created by Liu et al. [34] and has an ultra-high sensitivity (GF_{max} = 489.3) and a large strain range of up to 20%. A novel strain sensor with layered cracks built of Au/graphene composite film was proposed by Gong et al. [35], and it demonstrated great sensitivity (GF≈153) and favorable linearity (R^2≈0.9975) in the broad working range (0–20%). Ag/LIG strain sensors with great sensitivity(GF = 223.6) and a wide operating range(70%–100%) were created by Xie et al. [36] By adding rare metals to LIG, the electromechanical characteristics are enhanced, but the cost is also raised.

Due to their layered structures and tunable characteristics, transition metal dichalcogenides (TMDs) have garnered a lot of attention in the past ten years as potential materials for flexible electronics [37,38]. Especially, molybdenum disulfide (MoS_2) is one of the candidates in high-performance flexible strain sensors owing to its excellent mechanical properties [39]. Park's team [40] proposed highly sensitive strain sensors (GF≈1242) based on MoS_2-decorated LIG. Its electromechanical properties are improved by taking advantage of the high mobility of graphene and the structural rigidity of MoS_2. In addition to MoS_2, hafnium diselenide ($HfSe_2$) is a particularly interesting member, because it shows a moderate band gap and outstanding mechanical properties. The Young's modulus, fracture strength, and maximal strain of $HfSe_2$ were recently measured to be ~ 39.3 ± 8.9 Gpa, 4.5 ± 1.4 GPa, and 14.0–20.9%, respectively, [41] which far exceeds the stretchability of other 2D materials including MoS_2 [42]. And hafnium oxide (HfO_2) prepared by laser irradiation of the $HfSe_2$ surface exhibits a higher Yang's modulus (182.6 ± 54.3 GPa) [41]. $HfSe_2$ is appealing in strain sensors due to its exceptional elasticity, excellent electrical and photoelectric properties. However, because there has been little research on $HfSe_2$ flexible strain sensors, this work investigates a stretchable strain sensor based on $HfSe_2$/LIG.

Herein, we proposed a simple method for fabricating $HfSe_2$ embedded LIG porous composite ($HfSe_2$/LIG) for use in wearable strain sensors. Three-dimensional porous graphene with $HfSe_2$ decorations was created by irradiating a multilayer $HfSe_2$ coating on a commercial PI film with a CO_2 infrared laser, which produces superior electromechanical properties. According to the experimental results, the $HfSe_2$/LIG composite material on Ecoflex substrate exhibits high sensitivity (GF ≈ 46) and good linearity (R^2 = 0.99) over a wide tensile range (0–30%). When under strain conditions of 30–50%, GF_{max} ≈ 150. And it has high tensile durability (>3000 cycles). Further evidence of their broad potential for use in wearable electronics comes from the fact that reliable signals can be picked up from a variety of human body motion-monitoring tests (such as those performed on the fingers, wrists, and neck) as well as subtle pulse perception.

2. Experimental section

2.1. The production process of $HfSe_2$ solution

$HfSe_2$ solution was made by mixing 5 ml of ethanol (anhydrous, 99.8%, Sigma Aldrich) solvent with 10 mg of hafnium diselenide powder ($HfSe_2$, purchased from Shenzhen Six Carbon Technology). The obtained mixture was immersed in an SBL-15DT benchtop ultrasonic bath (400 W) for 12 h at a frequency of 40 kHz and 100% power sonication. During sonication, the bath temperature was kept below 30 °C by a water-cooled circulating pump. The $HfSe_2$ ethanol dispersion was obtained, the upper layer was taken, spray-coated on the surface of a 100 μm polyimide film (PI film), and the solvent was then evaporated in a blast drying oven at 80 °C for 30 min.

2.2. Fabrication of $HfSe_2$/LIG strain sensor

The $HfSe_2$-coated PI film was irradiated with a CO_2 infrared laser. A 10.6 μm CO_2 laser with a maximum power of 40 W was used in this study. The final device was produced using the laser parameters that have been optimized, which have a power of 7% and a speed of 80 mm/min in ambient conditions.

Ecoflex 00–20 (Smooth-On) was used as the $HfSe_2$/LIG strain sensor substrate in this study, and its parts A and B were mixed in a weight ratio of 1:1 before being degassed and drop-cast onto the laser-patterned $HfSe_2$/LIG film (thickness about 0.5 mm). The PI film was then peeled off to realize the transfer of $HfSe_2$/LIG to the surface of the Ecoflex flexible substrate after the Ecoflex film had been cured at 80 °C for 4 h. Then, by joining $HfSe_2$/LIG patterns with copper wires, electrical contact was created with the aid of silver paste. Finally, Ecoflex suspension was used for the final encapsulation (thickness about 0.5 mm), creating a completely flexible strain sensor.

2.3. Materials characterizations and electromechanical measurement

The surface morphology of the $HfSe_2$/LIG network was examined using scanning electron microscope (SEM, Gemini 300, Zeiss) images for material characterization. The same instrument was also used to conduct energy dispersive X-ray spectroscopy (EDS) for elemental analysis. By using LabRAM HR Evolution (HORIBA) and a 532 nm laser to excite it, Raman spectrum was obtained. X-ray photoelectron spectroscopy (XPS) spectra of $HfSe_2$/LIG were also measured. The XPS analyses were carried out on a PHI 5000 VersaProbe III spectrometer using monochromatic Al(alpha) X-ray source (hv = 1486.6 eV). The analyzer pass energy is selected as 280.0 eV and step size of 1.0 eV. High resolution analyses were carried out with same X-ray settings and analysis area, while analyzer pass energy is selected at 69.0 eV and step size of 0.125 eV. Spectra have been charge corrected to the main line of the C 1 s spectrum (adventitious carbon) and set to BE of 284.8 eV. The acquired data were analyzed using PHI MultiPak software. During element curve fitting, a "Shirley" background subtraction method is used and fitting curve line-shape had chosen to use the "Gaussian-Lorentzian" function. The lattice fringes and spacing of LIG and $HfSe_2$ were characterized using a field emission gun transmission electron microscope (TEM, Talos F200s) with energy dispersive spectrometer (EDS, SUPER X).

The static testing apparatus (Wance Instrumente) was used to apply longitudinal strain to the $HfSe_2$/LIG strain sensor during electromechanical testing. A multichannel data acquisition system (DAQ6510, Keithley) was utilized to record the resistance signal in real time during the stretching and releasing process. And a digital source meter (2450, Keithley) was applied to measure the I-V curve.

3. Results and discussion

3.1. Fabrication and characterization of $HfSe_2$/LIG strain sensor

Fig. 1a illustrates the fabrication process of the $HfSe_2$-decorated LIG ($HfSe_2$/LIG) strain sensor. Firstly, $HfSe_2$ dispersion was sprayed on PI film by a spray gun, which can reduce the surface tension of dispersion and make $HfSe_2$ cover the PI surface more evenly. Secondly, the film was treated with a 10.6 μm CO_2 laser to obtain $HfSe_2$/LIG. To increase the ductility and mechanical robustness, $HfSe_2$/LIG was transferred to the surface of the Ecoflex flexible substrate by infiltration method, and the Ecoflex-$HfSe_2$/LIG composite film was obtained. Video_S1 (Supporting Information) shows the surface robustness after transfer. Next, the copper wire was connected to the $HfSe_2$/LIG pattern through silver paste to make electrical contact. Finally, Ecoflex suspension was adopted in the encapsulation, thus forming a complete flexible strain sensor with a size of 25 mm × 5 mm, as shown in Fig. 1b. The sensor has good flexibility and stretchability. Fig. 1c shows the sensor after stretching at about 100% strain, and Fig. 1d shows the bending characteristics of the sensor.

The SEM image from Fig. 2a depicts the morphology and microstructure of $HfSe_2$/LIG on PI substrate (PI-$HfSe_2$/LIG). The results indicate that $HfSe_2$/LIG is a three-dimensional network structure, which is consistent with the results in the literature [23,34,40]. And $HfSe_2$ is dispersed on the surface of LIG, which is shown in Fig. 2b, and the elemental mapping of $HfSe_2$/LIG is shown in Fig. S1a, which reveals that the composites include C, Hf, Se and O atoms. After that, the surface is poured with Ecoflex liquid, and its fluidity will automatically fill into the three-dimensional network structure, which is conducive to the transfer of $HfSe_2$/LIG. The morphology of the transferred surface (Ecoflex-$HfSe_2$/LIG) is shown in Fig. S2b. And the cross-section SEM images (Fig. S2c-d) of $HfSe_2$/LIG on PI and Ecoflex substrate both show the thickness of $HfSe_2$/LIG is about 50 μm. The contact angle of $HfSe_2$/LIG on PI and Ecoflex substrate was also tested, respectively, as shown in Fig. S2e-f. The results indicate that $HfSe_2$/LIG surface changed from hydrophilic (contact angle of 52.68°) to hydrophobic (contact angle of 118.78°) after transferring to the Ecoflex substrate, thus improving the robustness and environmental stability of the $HfSe_2$/LIG strain sensor.

Raman spectra were measured to further characterize the chemical structure of $HfSe_2$/LIG. Fig. 2c depicts the Raman spectrum of PI-LIG, Ecoflex-LIG and PI-$HfSe_2$/LIG for analyzing their differences. Three typical characteristic peaks of LIG at ~ 1350, 1585 and 2700 cm^{-1} were identified in the above materials, and these peaks are consistent with the Raman spectra of typical LIG obtained by laser irradiation of PI films previously reported [23,34]. The above three typical characteristic peaks correspond to D peak (indicating that sp^2 carbon bond is defective or bent), G peak (showing the first-order scattering vibration of sp2 hybrid carbon atoms, suggesting graphitization), and 2D peak (related to the boundary phonons of the second-order region and determined by the number of graphene stacks), respectively [23,43]. Among them, the

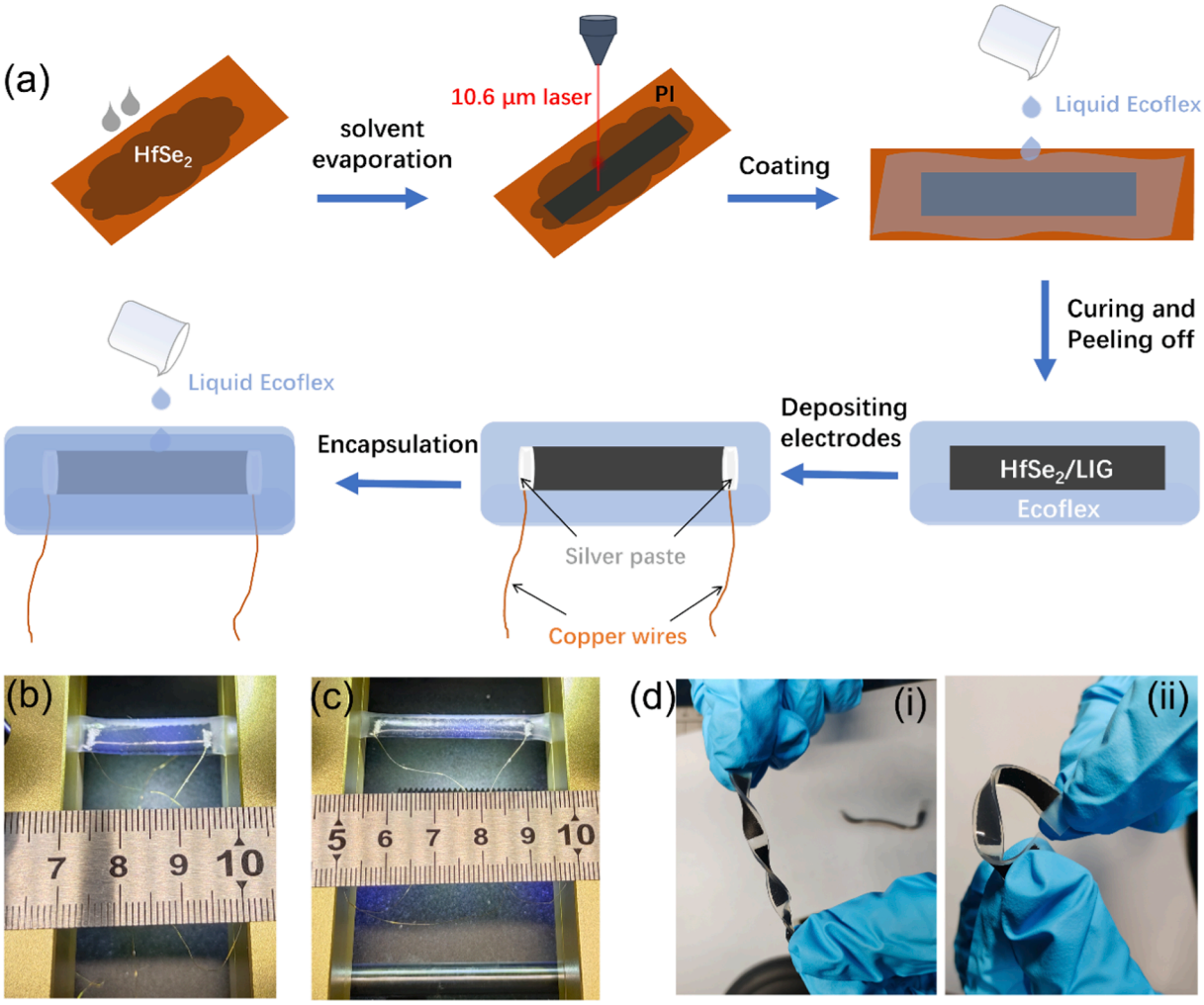

Fig. 1. Preparation process and device pictures of stretchable strain sensor based on $HfSe_2$/LIG. (a) Fabrication schematic diagram of resistive flexible strain sensor based on $HfSe_2$/LIG. (b)-(c) Photographs show the final strain sensor with a size of 25 mm × 5 mm at 0% and 100% strain, respectively. (d) Photographs show the bending characteristics of the sensor.

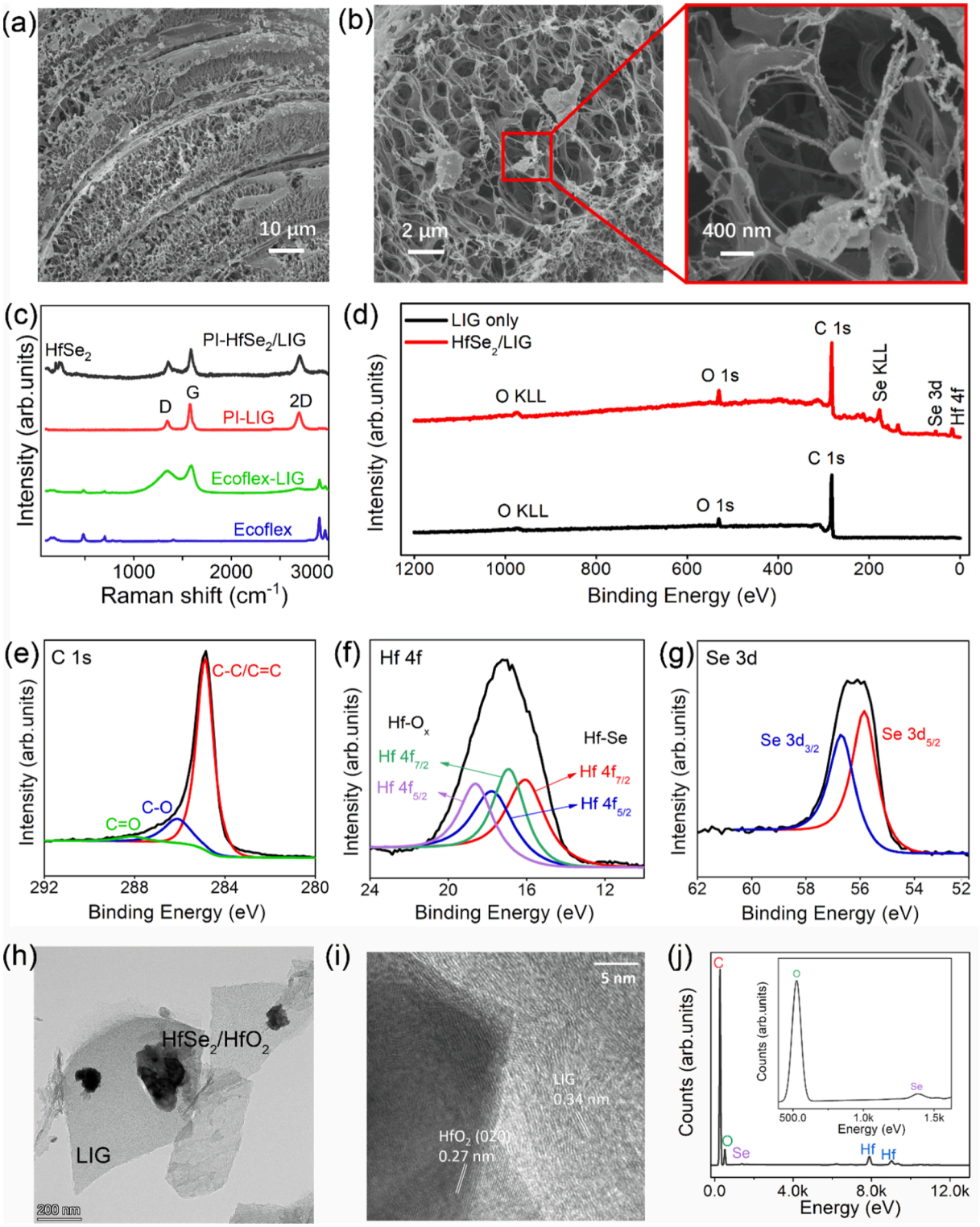

Fig. 2. Characterization and analysis of $HfSe_2$/LIG composites. (a)-(b) Morphology and microstructure of $HfSe_2$/LIG on PI substrate. (c) Raman spectrum of PI-LIG, Ecoflex-LIG, and PI-$HfSe_2$/LIG. (d) The full XPS spectra of $HfSe_2$/LIG composites and LIG-only. (e) The XPS spectrum of C 1s, indicating that the C–C peak of LIG in the $HfSe_2$/LIG composite is the main part. (f) The XPS spectrum of Hf 4f. (g) The XPS spectrum of Se 3d. (h) Low-magnification TEM image of $HfSe_2$/LIG. (i) HRTEM image of $HfSe_2$/LIG. (j) EDS spectrum of the $HfSe_2$/LIG.

Raman spectrum of Ecoflex-LIG shows that the FWHM (Full width at half maximum) of G and D peaks increases, and the intensity of 2D peaks decreases. This is because after transferring, the graphite at the bottom turns to the surface [31,44]. In magnified Raman spectra of PI-$HfSe_2$/LIG (Fig. S1b), $HfSe_2$-related peaks at 199 cm^{-1} were also observed at low wavenumbers, which is the A_{1g} mode and arises from the out-of-plane vibration of Se atoms [45–47]. The other characteristic peaks located at 237 cm^{-1} and 257 cm^{-1} were also identified, which are derived from selenium (Se) [48]. This is because the laser partially oxidizes the top layers of $HfSe_2$, forming $HfSe_xO_y$ and precipitating Se [45].

The chemical composition and bonding type of $HfSe_2$/LIG composites were researched by X-ray photoelectron spectroscopy (XPS). The full XPS spectrum of LIG and $HfSe_2$/LIG are both shown in Fig. 2d, which further confirms that the elemental composition of $HfSe_2$/LIG is C, O, Hf and Se atoms, and their chemical states. Furthermore, high-resolution XPS spectrum of the C 1s region (Fig. 2e) shows that the C–C peak is centered at 284.6 eV, which is distinctive of the graphene structure [49]. Fig. 2f shows the Hf-Se bonding (Hf $4f_{5/2}$ and $4f_{7/2}$) peaks of $HfSe_2$/LIG samples located at 17.87 and 16.12 eV, respectively. And other two Hf peaks are located at 18.60 and 16.87 eV, corresponding to the Hf-O bonds of air-exposed $HfSe_2$ [45,50]. When fitting the Hf 4f peak, the constraints of the features settings such as FWHM, spin orbit splitting, and relative intensity are shown in Supporting information. And we observed Se $3d_{3/2}$ (56.72 eV) and Se $3d_{5/2}$ (55.85 eV) for Se-Se bonding, [50,51] as shown in Fig. 2g. In Fig. 2h, the TEM image of $HfSe_2$/LIG confirms that $HfSe_2$ nanoparticles are uniformly modified on several layers of LIG, where 0.34 nm lattice spacing is allocated to the (002) plane of graphene, and 0.27 nm lattice spacing is allocated to the (020) plane of HfO_2 nanoparticles generated after $HfSe_2$ surface oxidation (Fig. 2i). [23] In Fig. 2j, the EDS spectra of C, O, Hf, and Se elements indicate the presence of $HfSe_2$ nanoparticles on LIG. However, due to the high temperature generated during laser manufacturing, a large amount of surface oxidation occurred, resulting in the generation of HfO_2. Therefore, the above results show that the surface layer of $HfSe_2$ can be partially oxidized by laser irradiation.

3.2. *Electromechanical performance of the $HfSe_2$/LIG strain sensor*

In this part, the electromechanical performance of $HfSe_2$/LIG strain sensor need to be tested and evaluated, so the in-situ experimental platform was built and described in detail in the Experimental Section.

As can be seen in Fig. 3a, the electromechanical performance was evaluated initially to see how tensile frequency affected it. The relative resistance change ($\Delta R/R_0$) is nearly the same when stretching 4 mm (10% strain) at various stretching rates (1 mm/s, 2 mm/s, 4 mm/s, 5 mm/s, and 7 mm/s), proving that the device is unaffected by the stretching frequency.

Additionally, the $HfSe_2$/LIG strain sensor's current–voltage (I-V) properties under various strains were studied. As seen in Fig. 3b, the current follows Ohm's law's linear relationship and rises monotonically as the bias voltage rises. Meanwhile, the slope of the I-V curve flattens out as the strain increases, supporting the piezoresistive characteristics of the $HfSe_2$/LIG strain sensor.

The GF (gauge factor) was determined using the following calculation to assess the sensitivity of the $HfSe_2$/LIG strain sensor and compare it to other sensors:

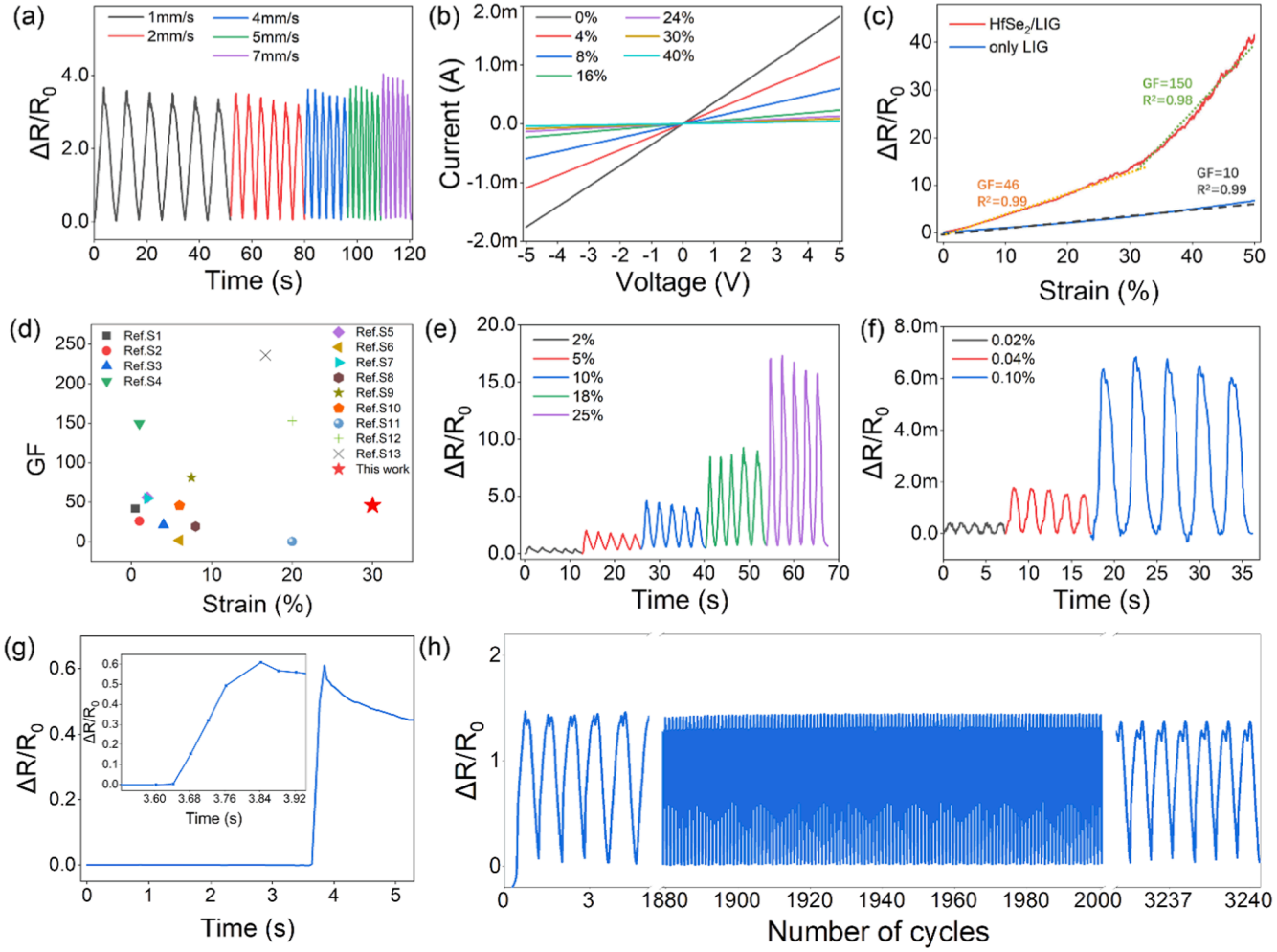

Fig. 3. The electromechanical properties of the $HfSe_2$/LIG strain sensor. (a) Effects of different stretching frequencies on electromechanical responses of $HfSe_2$/LIG strain sensor. (b) I-V curves of $HfSe_2$/LIG strain sensor under different tensile strains (0–40%). (c) The comparison of GF between the $HfSe_2$/LIG strain sensor and LIG-only strain sensor. (d) Comparisons of $HfSe_2$/LIG strain sensor and recently reported stretchable strain sensors. (e) Time-dependent relative resistance change ($\Delta R/R_0$) of $HfSe_2$/LIG strain sensor to five continuous stretch/release cycles of 2%, 5%, 10%, 18% and 25% stretch strain. (f) Relative change in resistive response to 0–0.1%-0, 0–0.04%-0, 0–0.02%-0 cyclic strain used to determine the lower detection limit. (g) The response time of the $HfSe_2$/LIG strain sensor. (h) The electromechanical recyclability of $HfSe_2$/LIG strain sensor remains stable over 3000 cycles under 4% strain.

$$GF = \frac{\delta(\Delta R/R_0)}{\delta\varepsilon} = \frac{\delta((R-R_0)/R_0)}{\delta(\Delta L/L_0)} \quad (1)$$

where R is the resistance at a particular strain and R_0 is the initial resistance. The relative resistance change ($\Delta R/R_0$) of the sensor grows monotonically with the amount of applied tensile strain. Additionally, the slope of the $\Delta R/R_0$-ε curve, which plots the relative resistance change against tensile strain, was used to determine the strain sensitivity of the sensor.

In Fig. 3c, "$\Delta R/R_0$-ε" curve for the $HfSe_2$/LIG strain sensor indicates that it provides a GF of 46 with $R^2 = 0.99$ up to the strain of 30% and then increases to 150 with $R^2 = 0.98$ beyond 30%. A sensor made of LIG alone was also fabricated for performance comparison using the same process as the $HfSe_2$/LIG sensor. Fig. 3c illustrates that the GF of the $HfSe_2$/LIG strain sensor is higher than that of the LIG-only strain sensor. The $HfSe_2$/LIG sensor's strain sensing performance (GF of 46 and stretchability of 30%) is also comparable to stretchable strain sensors based on LIG/Pt (GF of 45.6 and stretchability of 6%), [34] graphene/Au (GF of 153 and stretchability of 20%), [35] LIG/MoS_2 (GF of 236.2 and stretchability of 16.7%) [40]. Table S1 compares the detailed strain sensing performance of our strain sensor with the recently reported high-performance strain sensor. Fig. 3d also depicts GFs and the first linear stretching range, illustrating that the $HfSe_2$/LIG sensor can provide high sensitivity and good linearity sensing over a broad stretching range.

We have provided a schematic description of the sensing mechanism based on experimental observations. Fig. 4a shows the surface formation process of the LIG/$HfSe_2$ sensor. The PI surface forms a characteristic 3D porous structure through laser radiation. Therefore, the liquid Ecoflex can penetrate into the porous structure and fill the micropores after crosslinking during the casting and stripping steps. After the PI is peeled off, LIG/$HfSe_2$ is brought to the surface. The surface morphology of LIG/$HfSe_2$ in this work is shown in Fig. 4b, which is determined by the laser scanning interval and laser scanning speed. When the LIG/$HfSe_2$ encounters external forces, stress concentration occurs in the mechanically weak area, which is the connection between adjacent laser points. Subsequently, many microcracks were generated, which can be further assembled into sensors with strain sensitivity, as shown in Fig. 4c. Fig. 4d-f also shows SEM images of the microstructure of $HfSe_2$/LIG composite material at different strain levels, further revealing the strain sensing mechanism of the sensor. The $HfSe_2$/LIG surface exhibits obvious cracks in its initial state, as shown in Fig. 4d, which is caused by tearing the $HfSe_2$/LIG during peeling off PI. At 20% strain (Fig. 4e), the original crack increases, while the LIG is still in contact; At the same time, new microcracks are generated, so the resistance increases. As the strain increases to 40% (Fig. 4f), the original crack width further increases and the LIG contact begins to weaken. And the new cracks are further increased, which leads to the further increase of the resistance value and the increase of GF. When the strain exceeds 60% (Fig. 4g), the original crack width significantly increases, leading to complete disconnection of LIG and sudden generation of infinite resistance, verifying the macroscopic change in resistance dominated by cracks.

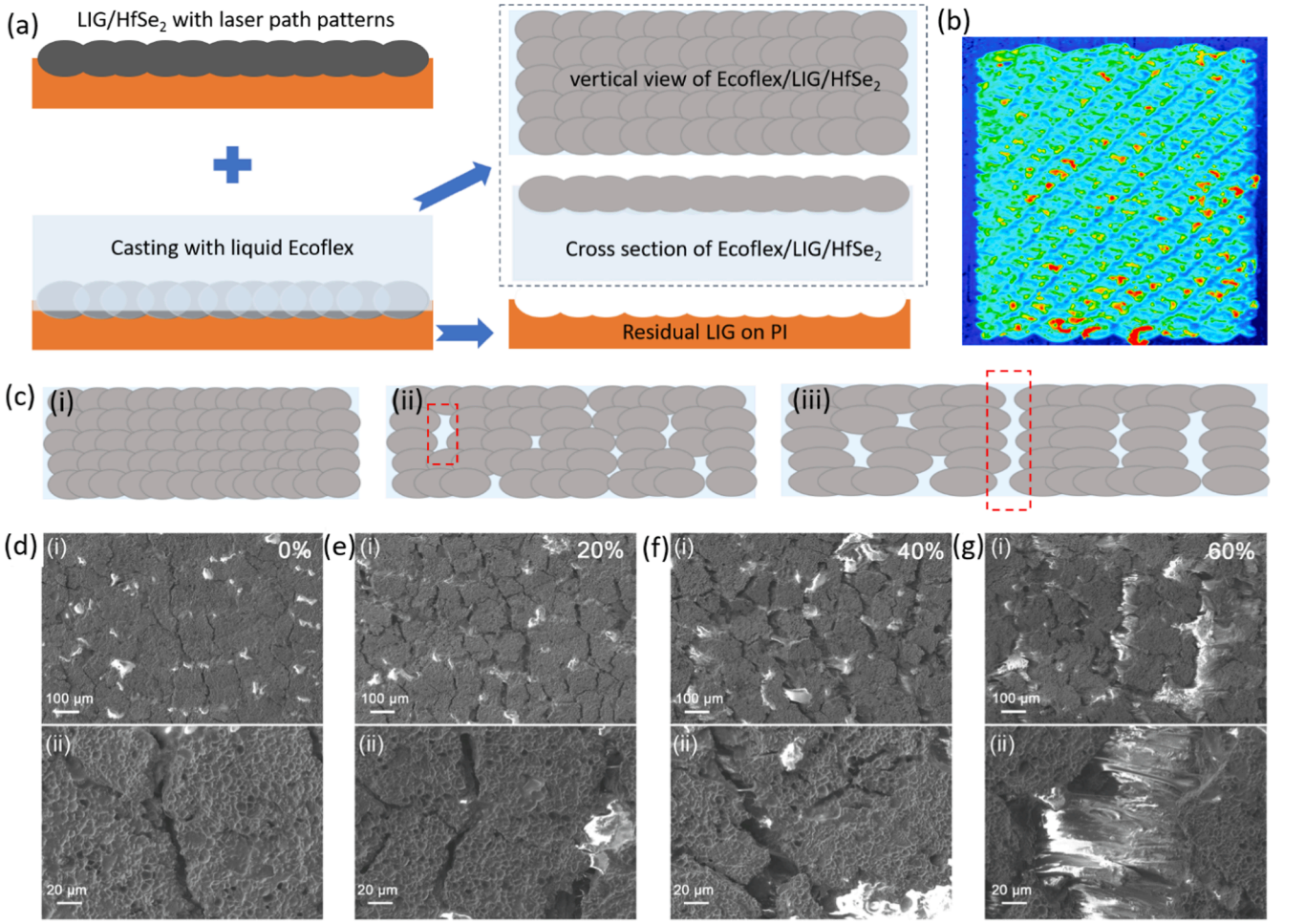

Fig. 4. (a) Schematic diagram of the cross-sectional morphology evolution of LIG/$HfSe_2$ in the casting and peeling process. (b) the 3D morphology map of LIG/$HfSe_2$ surface. (c) Schematic diagram of cracks in LIG/$HfSe_2$ sensors under various strains; The complete fracture of the crack occurs beyond the maximum strain (~50%). The SEM images of the $HfSe_2$/LIG composite microstructure at various applied strains: (d) 0%, (e) 20%, (f) 40%, and (g) 60%.

Additional studies were carried out to describe the dynamic behavior of the $HfSe_2$/LIG strain sensor. Fig. 3e shows the sensor's cyclic responses to relatively high strains of 2%, 5%, 10%, 18%, and 25%. The sensor keeps its initial resistance throughout each successive cycle, as seen in Fig. 3e, because the crack re-bridges after the applied strain is withdrawn. The primary cause of the high GF and reversible electrical connection is crack propagation. High sensitivity allowed for the benefit of examining the lower detection limit by continually observing the response while adding small amounts of strain. The sensor can detect a cyclic strain of 0%−0.02%−0%, as illustrated in Fig. 3f, which is close to the best value ever recorded [40,52]. As can be seen in Fig. 3f, the sensor performance was further examined for increasing strain levels of 0.04% (red line) and 0.1% (blue line). The findings demonstrate that under each strain condition, the relative change in resistance response is very good and fully recovers following release. Additionally, strains ranging from 4% to 20% were applied to the sensor to evaluate its dynamic response. The sensor was stretched and held for 5 s, then released and held for an additional 5 s as the resistance was recorded continuously, as seen in Fig. S3a. During applied strain, the sensor's response remains constant and returns to its eigenvalues upon release. Similarly, the sensor's staircase response was examined by sequentially stretching it by 4% strain and holding it for 5 s, as seen in Fig. S3b. And when it reached 28%, the strain was released in the same step size as stretching. The reactions to the stretching and releasing curves are symmetrical, but when releasing, there is an overshoot signal caused by the viscoelasticity of the flexible substrate [4]. Fig. 3g depicts dynamic response time of the sensor. The dynamic response time is determined by how fast the sensor reacts to strain loading. When the stretching speed was 7 mm/s (the maximum allowable stretching speed in this work), the time interval between adjacent horizontal shifts was observed as 0.20 s, indicating that the response after stretching is fast.

Furthermore, to assess the sensor's long-term durability, more than 3000 strain/release cycles (4% strain) were applied to test the electromechanical stability. The sensor responses did not differ significantly during the recycles test, as shown in Fig. 3h. After 3000 recycles, the device still performs well, effectively retaining its electromechanical properties. We discovered that even after 3000 electromechanical test cycles, the value of $\Delta R/R_0$ decreased from 1.44 to 1.36, indicating the sensor's long-term durability. To further verify the repeatability of the strain sensor, the surface morphology of the device was characterized by SEM after stretching for different cycles, with a stretching frequency of 1 Hz and a strain of 40%. From the SEM images of Figure S4, it can be seen that there is no significant difference in the surface crack morphology after 100, 500, 1000, and 2000 cycles of stretching, further demonstrating the stability and reliability of the device during repeated stretching. The excellent endurance of sensor is attributable to the capacity of crack repair during strain release to be reversed.

In addition to stretching, the sensing performance during pressing

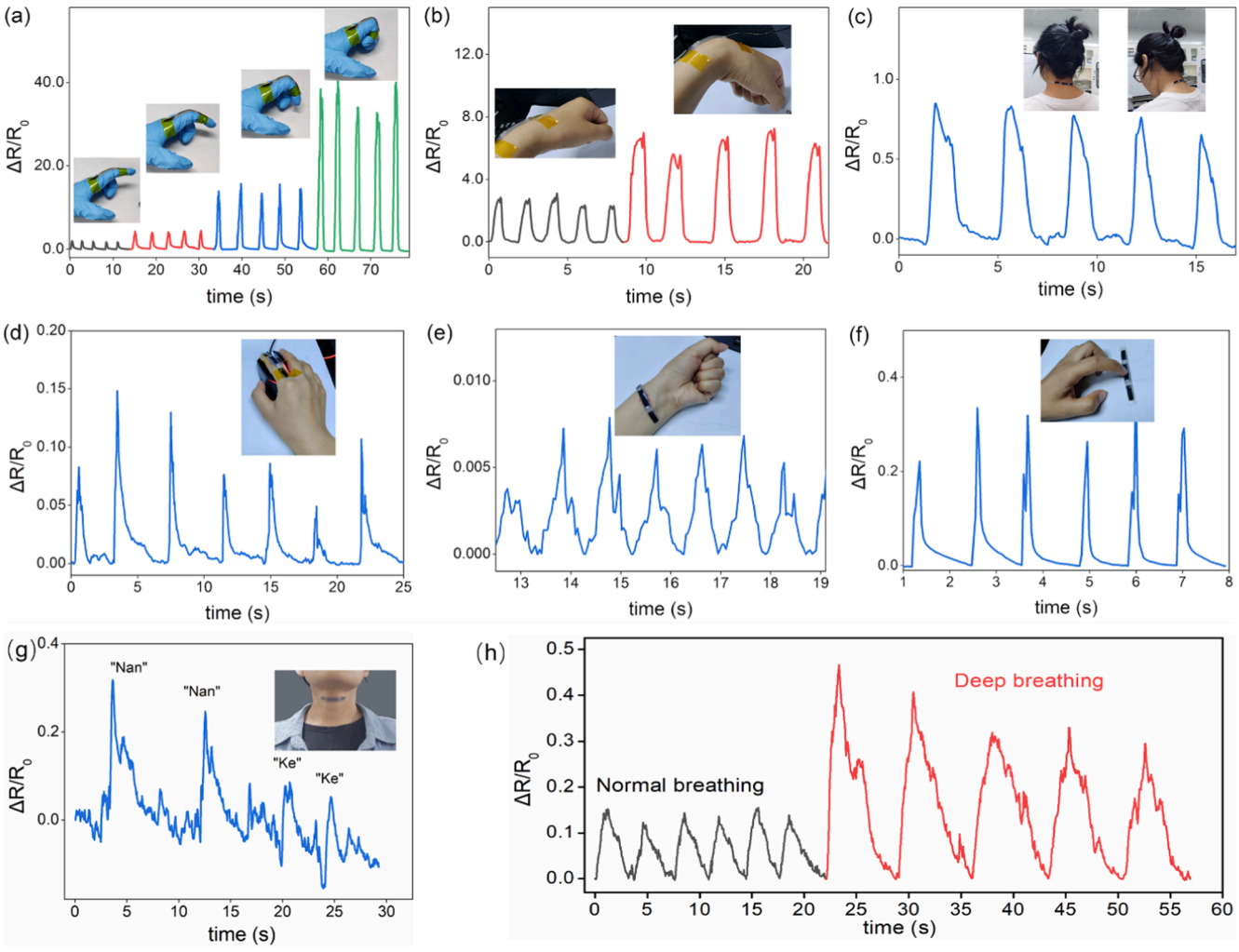

Fig. 5. The application of the $HfSe_2$/LIG device for various real-time signals. (a) Detect human motion by installing strain sensors on the finger joints. Relative changes in the resistive response of continuous bending/relaxation under different bending angles (30°, 60°, 90°, and 120°). (b) Relative resistance changes of the sensor when monitoring wrist bending. Relative resistance changes of the sensor when (c) the sensor is attached to the cervical spine, (d) the mouse is clicked, (e) testing wrist pulse, (f) pressing the sensor. (g) Relative resistance change of the sensor when the wearer spoke "Nan", "Ke". (h) Breathing test.

was also investigated. Fig. S3c depicts the device's response to pressure, and the value of $\Delta R/R_0$ increases as pressure increases, indicating that the $HfSe_2$/LIG sensor has attractive pressure monitoring capability.

3.3. Applications of the $HfSe_2$/LIG strain sensor

To demonstrate that the $HfSe_2$/LIG strain sensor, as a motion detector of an integrated health monitoring platform, can perceive a large number of joint-level and delicate skin-level strain signals, we place the sensors in various positions on the human body and track their reactions in real time.

For deformation caused by violent human motion, the sensor is fixed on the wrist and index finger joint by tightly wrapping bandages. The relative resistance response to various degrees of finger bending is shown in Fig. 5a. The sensor's resistance rises by approximately 180%, 410%, 1300%, and 3400% when the finger is bent by 30°, 60°, 90°, and 120°, respectively. When the sensor is mounted to the back of a person's wrist, as in Fig. 5b, it then exhibits a very steady resistance change to wrist bending. The above results show that $HfSe_2$/LIG strain sensor has great strain sensing ability and can be embedded in smart wearable devices for tracking human motion. Fig. 5c shows a highly reproducible and reversible resistance signal as it captures the sensor's resistance change in response to the volunteer bowing or raising her head, which indicates that it has great prospect in helping patients with cervical spondylosis rehabilitate.The test when a finger clicks the mouse is shown schematically in Fig. 5d, along with the associated $\Delta R/R_0$-time curve. At the top of this curve, the mouse is clicked by the finger, and at the bottom, the released state is represented. When the finger clicks the mouse, the skin of the finger is slightly deformed, and the sensor can sensitively detect this change.

For correct medical diagnosis, it is also crucial to accurately track respiration and blood circulation, therefore it is also required to keep an eye on minute physiological signs like wrist pulse. Similarly, it has been demonstrated that the $HfSe_2$/LIG sensor is sensitive enough to detect wrist pulsation. The result is shown in Fig. 5e. The graphic shows three distinctive peaks: the percussion peak (P), tidal peak (T), and diastolic peak (D). Other detection of subtle motion has also been tested. As expected, when the wearer utters different words such as "Nan" and "Ke", the $HfSe_2$/LIG strain sensor is connected to the throat to detect the vibration signal of the vocal cords (Fig. 5g). In addition, the sensor can also be used to monitor respiratory rate. As shown in Fig. 5h, different respiratory states can be distinguished by the amplitude, and frequency of the sensing signal, indicating the potential application of detecting subtle motion.

Furthermore, Fig. 5f shows the schematic diagram of the pressure test when finger pressing, and the corresponding $\Delta R/R_0$-time curve. The top of this curve is finger pressed, while the bottom stands for the released state, which shows that the sensor also has sufficient sensitivity to detect pressure.

4. Conclusion

In conclusion, $HfSe_2$/LIG composites were prepared in this work using a straightforward procedure. Three-dimensional porous graphene modified by $HfSe_2$ was synthesized by irradiating multilayer $HfSe_2$ coated on commercial PI films with CO_2 infrared laser. After being transferred to the flexible substrate of Ecoflex, it had high stretchability, hydrophobicity and robustness, and obtained excellent electromechanical properties. So, the electromechanical characteristics of $HfSe_2$/LIG strain sensor were examined. The $HfSe_2$/LIG strain sensor provides a GF of 46 with good linearity ($R^2 = 0.99$) in a broad tensile range (0–30%) and then increases to 150 with $R^2 = 0.98$ beyond 30%. The $HfSe_2$/LIG strain sensor demonstrated excellent sensitivity ($GF_{max} \approx 150$), low detection limit of 0.02% and great tensile durability (>3000 cycles). Its potential use as a wearable strain sensor is assessed in light of its exceptional sensing capabilities. The sensor can reliably pick up signals of minute artery activity as well as a variety of joint motions (including those of the fingers, wrists, and neck). The sensor based on $HfSe_2$/LIG has potential uses in wearable intelligent electronic devices, healthcare applications, and tracking human movements.

CRediT authorship contribution statement

Huiru Yang: Conceptualization, Investigation, Writing – original draft. **Shaogang Wang:** Methodology, Resources. **Qianming Huang:** Methodology, Visualization. **Chunjian Tan:** Formal analysis, Investigation. **Chenshan Gao:** Data curation, Visualization. **Siyuan Xu:** Investigation. **Huaiyu Ye:** Supervision, Funding acquisition, Writing – review & editing, Validation. **Guoqi Zhang:** Funding acquisition.

Declaration of Competing Interest

The authors declare that they have no known competing financial interests or personal relationships that could have appeared to influence the work reported in this paper.

Data availability

Data will be made available on request.

Acknowledgments

This work is supported by the Shenzhen Fundamental Research Program (JCYJ20200109140822796). Special Funds for the Cultivation of Guangdong College Students' Scientific and Technological Innovation (pdjh 2022c0080).

Appendix A. Supplementary material

Supplementary data to this article can be found online at https://doi.org/10.1016/j.apsusc.2023.157772.

References

[1] Z. Shen, F. Liu, S. Huang, H. Wang, C. Yang, T. Hang, J. Tao, W. Xia, X. Xie, Progress of flexible strain sensors for physiological signal monitoring, Biosens. Bioelectron. 211 (2022), 114298.
[2] S. Li, X. Xiao, J. Hu, M. Dong, Y. Zhang, R. Xu, X. Wang, J. Islam, Recent Advances of Carbon-Based Flexible Strain Sensors in Physiological Signal Monitoring, ACS Appl. Electron. Mater. 2 (2020) 2282–2300.
[3] Y. Lu, M.C. Biswas, Z. Guo, J.W. Jeon, E.K. Wujcik, Recent developments in bio-monitoring via advanced polymer nanocomposite-based wearable strain sensors, Biosens. Bioelectron. 123 (2019) 167–177.
[4] M. Amjadi, K.-U. Kyung, I. Park, M. Sitti, Stretchable, Skin-Mountable, and Wearable Strain Sensors and Their Potential Applications: A Review, Adv. Funct. Mater. 26 (2016) 1678–1698.
[5] H. Kim, Y.T. Kwon, H.R. Lim, J.H. Kim, Y.S. Kim, W.H. Yeo, Recent Advances in Wearable Sensors and Integrated Functional Devices for Virtual and Augmented Reality Applications, Adv. Funct. Mater. 31 (2020).
[6] S. Pyo, J. Lee, K. Bae, S. Sim, J. Kim, Recent Progress in Flexible Tactile Sensors for Human-Interactive Systems: From Sensors to Advanced Applications, Adv. Mater. 33 (2021) e2005902.
[7] J.C. Yang, J. Mun, S.Y. Kwon, S. Park, Z. Bao, S. Park, Electronic Skin: Recent Progress and Future Prospects for Skin-Attachable Devices for Health Monitoring, Robotics, and Prosthetics, Adv Mater 31 (2019) e1904765.
[8] L. Wang, K. Jiang, G. Shen, Wearable, Implantable, and Interventional Medical Devices Based on Smart Electronic Skins, Advanced Materials Technologies 6 (2021).
[9] M. Amjadi, A. Pichitpajongkit, S. Lee, S. Ryu, I. Park, Highly Stretchable and Sensitive Strain Sensor Based on Silver Nanowire-Elastomer Nanocomposite, ACS Nano 8 (2014) 5154–5163.
[10] B.U. Hwang, J.H. Lee, T.Q. Trung, E. Roh, D.I. Kim, S.W. Kim, N.E. Lee, Transparent Stretchable Self-Powered Patchable Sensor Platform with Ultrasensitive Recognition of Human Activities, ACS Nano 9 (2015) 8801–8810.
[11] M. Chao, Y. Wang, D. Ma, X. Wu, W. Zhang, L. Zhang, P. Wan, Wearable MXene nanocomposites-based strain sensor with tile-like stacked hierarchical microstructure for broad-range ultrasensitive sensing, Nano Energy 78 (2020).
[12] J.W. Chen, Q.L. Yu, X.H. Cui, M.Y. Dong, J.X. Zhang, C. Wang, J.C. Fan, Y.T. Zhu, Z.H. Guo, An overview of stretchable strain sensors from conductive polymer nanocomposites, J. Mater. Chem. C 7 (2019) 11710–11730.

[13] C. Park, M.S. Kim, H.H. Kim, S.-H. Sunwoo, D.J. Jung, M.K. Choi, D.-H. Kim, Stretchable conductive nanocomposites and their applications in wearable devices, Appl. Phys. Rev. 9 (2022).
[14] M. Jian, C. Wang, Q. Wang, H. Wang, K. Xia, Z. Yin, M. Zhang, X. Liang, Y. Zhang, Advanced carbon materials for flexible and wearable sensors, Sci. China Mater. 60 (2017) 1026–1062.
[15] L. Wen, F. Li, H.M. Cheng, Carbon Nanotubes and Graphene for Flexible Electrochemical Energy Storage: from Materials to Devices, Adv. Mater. 28 (2016) 4306–4337.
[16] N.S. Lu, C. Lu, S.X. Yang, J. Rogers, Highly Sensitive Skin-Mountable Strain Gauges Based Entirely on Elastomers, Adv. Funct. Mater. 22 (2012) 4044–4050.
[17] T. Yamada, Y. Hayamizu, Y. Yamamoto, Y. Yomogida, A. Izadi-Najafabadi, D. N. Futaba, K. Hata, A stretchable carbon nanotube strain sensor for human-motion detection, Nat. Nanotechnol. 6 (2011) 296–301.
[18] Z.Y. Liu, D.P. Qi, P.Z. Guo, Y. Liu, B.W. Zhu, H. Yang, Y.Q. Liu, B. Li, C.G. Zhang, J. C. Yu, B. Liedberg, X.D. Chen, Thickness-Gradient Films for High Gauge Factor Stretchable Strain Sensors, Adv. Mater. 27 (2015) 6230–6237.
[19] H. Zhang, R. He, Y. Niu, F. Han, J. Li, X. Zhang, F. Xu, Graphene-enabled wearable sensors for healthcare monitoring, Biosens. Bioelectron. 197 (2022), 113777.
[20] Q. Zheng, J.-H. Lee, X. Shen, X. Chen, J.-K. Kim, Graphene-based wearable piezoresistive physical sensors, Mater. Today 36 (2020) 158–179.
[21] J. Han, J.Y. Lee, J. Lee, J.S. Yeo, Highly Stretchable and Reliable, Transparent and Conductive Entangled Graphene Mesh Networks, Adv. Mater. 30 (2018).
[22] Y. He, D. Wu, M. Zhou, Y. Zheng, T. Wang, C. Lu, L. Zhang, H. Liu, C. Liu, Wearable Strain Sensors Based on a Porous Polydimethylsiloxane Hybrid with Carbon Nanotubes and Graphene, ACS Appl. Mater. Interfaces 13 (2021) 15572–15583.
[23] J. Lin, Z. Peng, Y. Liu, F. Ruiz-Zepeda, R. Ye, E.L. Samuel, M.J. Yacaman, B. I. Yakobson, J.M. Tour, Laser-induced porous graphene films from commercial polymers, Nat. Commun. 5 (2014) 5714.
[24] T.S.D. Le, H.P. Phan, S. Kwon, S. Park, Y. Jung, J. Min, B.J. Chun, H. Yoon, S.H. Ko, S.W. Kim, Y.J. Kim, Recent Advances in Laser-Induced Graphene: Mechanism, Fabrication, Properties, and Applications in Flexible Electronics, Advanced Functional Materials, DOI 10.1002/adfm.202205158(2022).
[25] W. Wang, L. Lu, Z. Li, Y. Xie, Laser induced 3D porous graphene dots: Bottom-up growth mechanism, multi-physics coupling effect and surface wettability, Appl. Surf. Sci. 592 (2022).
[26] L. Lu, D. Zhang, Y. Xie, H. He, W. Wang, Laser Induced Graphene/Silicon Carbide: Core-Shell Structure, Multifield Coupling Effects, and Pressure Sensor Applications, Advanced Materials Technologies 7 (2022).
[27] J. Zhu, X. Huang, W. Song, Physical and Chemical Sensors on the Basis of Laser-Induced Graphene: Mechanisms, Applications, and Perspectives, ACS Nano 15 (2021) 18708–18741.
[28] L. Huang, J. Su, Y. Song, R. Ye, Laser-Induced Graphene: En Route to Smart Sensing, Nanomicro Lett 12 (2020) 157.
[29] W. Liu, Y. Huang, Y. Peng, M. Walczak, D. Wang, Q. Chen, Z. Liu, L. Li, Stable Wearable Strain Sensors on Textiles by Direct Laser Writing of Graphene, ACS Applied Nano Materials 3 (2020) 283–293.
[30] B. Kulyk, B.F.R. Silva, A.F. Carvalho, S. Silvestre, A.J.S. Fernandes, R. Martins, E. Fortunato, F.M. Costa, Laser-Induced Graphene from Paper for Mechanical Sensing, ACS Appl. Mater. Interfaces 13 (2021) 10210–10221.
[31] D.X. Luong, K. Yang, J. Yoon, S.P. Singh, T. Wang, C.J. Arnusch, J.M. Tour, Laser-Induced Graphene Composites as Multifunctional Surfaces, ACS Nano 13 (2019) 2579–2586.
[32] Y. Wu, I. Karakurt, L. Beker, Y. Kubota, R. Xu, K.Y. Ho, S. Zhao, J. Zhong, M. Zhang, X. Wang, L. Lin, Piezoresistive stretchable strain sensors with human machine interface demonstrations, Sens. Actuators, A 279 (2018) 46–52.
[33] A. Dallinger, K. Keller, H. Fitzek, F. Greco, Stretchable and Skin-Conformable Conductors Based on Polyurethane/Laser-Induced Graphene, ACS Appl. Mater. Interfaces 12 (2020) 19855–19865.
[34] W. Liu, Q. Chen, Y. Huang, D. Wang, L. Li, Z. Liu, In situ laser synthesis of Pt nanoparticles embedded in graphene films for wearable strain sensors with ultra-high sensitivity and stability, Carbon 190 (2022) 245–254.
[35] X. Cheng, J. Cai, J. Xu, Gong, High-Performance Strain Sensors Based on Au/Graphene Composite Films with Hierarchical Cracks for Wide Linear-Range Motion Monitoring, ACS Appl. Mater. Interfaces 14 (2022) 39230–39239.
[36] W. Wang, L. Lu, X. Lu, Z. Liang, H. Lin, Z. Li, X. Wu, L. Lin, Y. Xie, Scorpion-inspired dual-bionic, microcrack-assisted wrinkle based laser induced graphene-silver strain sensor with high sensitivity and broad working range for wireless health monitoring system, Nano Research, DOI 10.1007/s12274-022-4680-0 (2022).
[37] D. Jiang, Z. Liu, Z. Xiao, Z. Qian, Y. Sun, Z. Zeng, R. Wang, Flexible electronics based on 2D transition metal dichalcogenides, J. Mater. Chem. A 10 (2022) 89–121.
[38] L. Zheng, X. Wang, H. Jiang, M. Xu, W. Huang, Z. Liu, Recent progress of flexible electronics by 2D transition metal dichalcogenides, Nano Res. 15 (2021) 2413–2432.
[39] M. Zhu, X. Du, S. Liu, J. Li, Z. Wang, T. Ono, A review of strain sensors based on two-dimensional molybdenum disulfide, J. Mater. Chem. C 9 (2021) 9083–9101.
[40] A. Chhetry, M. Sharifuzzaman, H. Yoon, S. Sharma, X. Xuan, J.Y. Park, MoS2-Decorated Laser-Induced Graphene for a Highly Sensitive, Hysteresis-free, and Reliable Piezoresistive Strain Sensor, ACS Appl. Mater. Interfaces 11 (2019) 22531–22542.
[41] Y.M. Jahn, A. Ya'akobovitz, Outstanding stretchability and thickness-dependent mechanical properties of 2D HfS2, HfSe2, and hafnium oxide, Nanoscale 13 (2021) 18458–18466.
[42] S. Bertolazzi, J. Brivio, A. Kis, Stretching and Breaking of Ultrathin MoS2, ACS Nano 5 (2011) 9703–9709.
[43] A.C. Ferrari, J.C. Meyer, V. Scardaci, C. Casiraghi, M. Lazzeri, F. Mauri, S. Piscanec, D. Jiang, K.S. Novoselov, S. Roth, A.K. Geim, Raman spectrum of graphene and graphene layers, Phys. Rev. Lett. 97 (2006), 187401.
[44] K. Nagata, K. Ishibashi, Y. Miyamoto, Raman and Infrared Spectra of Rhombohedral Selenium, Jpn. J. Appl. Phys. 20 (1981) 463–469.
[45] L. Liu, Y. Li, X. Huang, J. Chen, Z. Yang, K.H. Xue, M. Xu, H. Chen, P. Zhou, X. Miao, Low-Power Memristive Logic Device Enabled by Controllable Oxidation of 2D HfSe2 for In-Memory Computing, Adv Sci (Weinh) 8 (2021) e2005038.
[46] L. Yin, K. Xu, Y. Wen, Z. Wang, Y. Huang, F. Wang, T.A. Shifa, R. Cheng, H. Ma, J. He, Ultrafast and ultrasensitive phototransistors based on few-layered HfSe2, Appl. Phys. Lett. 109 (2016).
[47] M. Kang, S. Rathi, I. Lee, D. Lim, J. Wang, L. Li, M.A. Khan, G.-H. Kim, Electrical characterization of multilayer HfSe2 field-effect transistors on SiO2 substrate, Appl. Phys. Lett. 106 (2015).
[48] A. Cruz, Z. Mutlu, M. Ozkan, C.S. Ozkan, Raman investigation of the air stability of 2H polytype HfSe2 thin films, MRS Commun. 8 (2018) 1191–1196.
[49] W. Wang, L. Lu, Z. Li, L. Lin, Z. Liang, X. Lu, Y. Xie, Fingerprint-Inspired Strain Sensor with Balanced Sensitivity and Strain Range Using Laser-Induced Graphene, ACS Appl. Mater. Interfaces 14 (2022) 1315–1325.
[50] M. Kang, S. Rathi, I. Lee, L. Li, M.A. Khan, D. Lim, Y. Lee, J. Park, S.J. Yun, D. H. Youn, C. Jun, G.H. Kim, Tunable electrical properties of multilayer HfSe2 field effect transistors by oxygen plasma treatment, Nanoscale 9 (2017) 1645–1652.
[51] G. Mirabelli, C. McGeough, M. Schmidt, E.K. McCarthy, S. Monaghan, I.M. Povey, M. McCarthy, F. Gity, R. Nagle, G. Hughes, A. Cafolla, P.K. Hurley, R. Duffy, Air sensitivity of MoS2, MoSe2, MoTe2, HfS2, and HfSe2, J. Appl. Phys. 120 (2016).
[52] Y. Ma, Z. Li, J. Han, L. Li, M. Wang, Z. Tong, J. Suhr, L. Xiao, S. Jia, X. Chen, Vertical Graphene Canal Mesh for Strain Sensing with a Supereminent Resolution, ACS Appl. Mater. Interfaces 14 (2022) 32387–32394.